BENCH TEST OF A FULL-SCALE ACTIVE TWIST BLADE SEGMENT

S. Opitz[1*], T. J. Adam[1], S. Kalow[1], P. Wierach[1],
[1]Institute of Composite Structures and Adaptive Systems, DLR (German Aerospace Center), Lilienthalplatz 7, 38108 Braunschweig, Germany

Abstract

The design, manufacturing and testing of a full scale active twist blade segment is presented. Customized coupon tests for material characterization establish the basis for the optimization of the design of a full scale active twist blade. A complex multiaxial bench test is developed to prove the durability of the blade structure and in particular of the piezoceramic actuators under fatigue loading. Analyzing the measurement results it is demonstrated that the derived blade design enables the integrated piezoceramic actuators to sustain the cyclic loading at all load levels up to limit load without failure. Only a minor decrease of active performance is observed that can be compensated since there is enough performance margin available.

1. INTRODUCTION

The main rotor of a helicopter is one of the major sources of noise and vibration for this type of aircraft. Furthermore the generation of noise and vibration is strongly depending on the flight condition of the helicopter [1]-[3]. Active twist blades have the potential to significantly reduce noise and vibration generated by the main rotor of a helicopter.

In decent flight noise is generated by blade vortex interactions [4]. Already small angles of ± 2 ° tip twist are sufficient to significantly reduce the noise carpet underneath the aircraft [5]-[7]. This noise reduction is caused by an increase in miss distance between vortex and blade. The effect relies on the modification of both the vortex trajectory and the blade position [8].

In fast forward flight major sources of noise and vibration are transonic effects and dynamic stall [9]. The amplitudes that are needed for vibration reduction are even smaller [5][7].

The active twist principle is currently intensively investigated using scaled rotor blades [10]-[18], however only a few studies focusing on full scale realization and upscaling of the technology have been done [19].

From a structural point of view, scaling down a rotor blade to model scale is quite complicated. Especially in case of Mach-scaled model rotors the combination of much higher centrifugal accelerations and confined space is not an easy task. Vice versa, scaling up state of the art piezoelectric actuators in order to fulfill the requirements for twisting a full scale blade is not less challenging. Especially the actuators are a crucial point that can limit the fatigue life of active rotor blades.

2. ACTUATORS

The currently used piezoceramic actuators are not monolithic. The so called Macro Fiber Composite Actuators (MFC) rather have a quite complex inner structure (see FIGURE 1) [20].

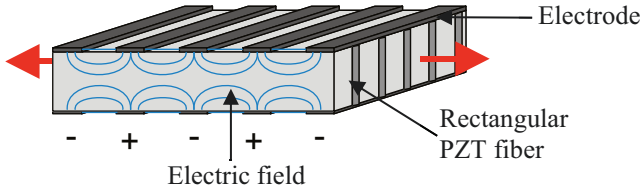

FIGURE 1. Macro Fiber Composite structure

They consist of rectangular piezoelectric fibers that have interdigitated electrodes on their top and bottom surface. Comparable to a flexible circuit board these electrodes are located on the surface of thin polyimide films.

The polyimide films encapsulate the piezoceramic material and form a mechanically more robust and electrically insulated piezoelectric composite.

The electric field that develops when different potentials are applied to the electrodes penetrates into the piezoceramic material and causes the fibers to extend in their longitudinal direction. The resulting electric field is not homogeneous. This causes areas directly underneath the electrodes that are not contributing to the strain generation of the actuator. Consequently the fiber thickness cannot be increased independently from the electrode spacing. As the generated strain depends on the strength of the electric field larger electrode spacing would need higher operating voltages to generate the same field strength and finally the same amount of actuator performance. Since the operating voltage of those actuators is already up to 1500 V a further increase is not favored.

Novel developed multilayer composite actuators have the potential to overcome these drawbacks [21][22]. So far they have only been tested in model scale rotor blades [23].

For this reason an active twist blade design with 3 MFC actuator layers is selected within the present study. The actuators are integrated into the blade skin and generate strain in ±45 ° direction referred to the blade longitudinal axis. The induced strain is oriented in the principle strain direction of torsion and therefore results in the intended blade twist. The stacking of actuators constrains the

*Corresponding author: Steffen.Opitz@dlr.de

accessibility to actuators in deeper layers. This inhibits conventional repair procedures and further emphasizes the need for long term stability and a high fatigue life of the actuators.

Due to the brittleness of the piezoceramic material used in those actuators, especially tensile strains (e.g. from centrifugal forces) establish a critical loading condition. During the intense testing of model scale blades different failure modes have been observed.

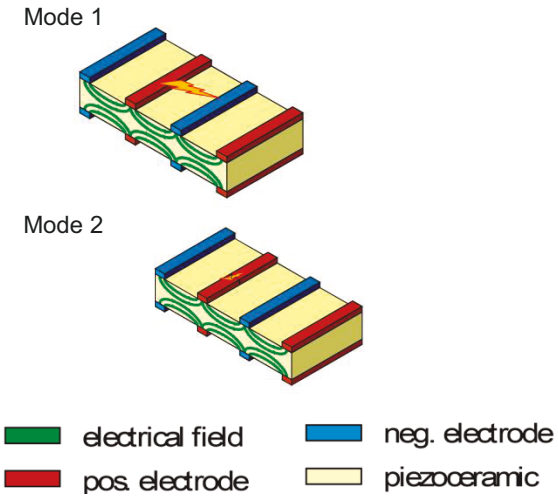

FIGURE 2. MFC failure modes

The first failure mode is characterized by a breakdown of the electrical insulation between positive and negative electrode. Usually an electric arc develops that melts or vaporizes the surrounding materials. After the failure the spot can be conductive or self-insulated. This determines whether further repair is needed or not. If this kind of failure occurs within a laminate with multiple actuator layers there is no possibility for a repair and it is likely that the whole actuator fails immediately.

The second failure mode is a crack within one electrode. These cracks are usually initiated by cracks in the piezoceramic material underneath. A crack in the piezoceramic fiber leads to high local strains within the electrode. Under fatigue loading the electrodes fail due to local strain hardening which makes them more brittle. When the actuators are operated regardless of the damage small electric arcs can be observed underneath the polyimide foil. These arcs form between fragments of the same electrode and therefore release much less energy than arcs between electrodes of different polarity. Nevertheless the actuator performance reduces and higher currents have to be driven by the amplifiers that operate the MFCs. Up to now there is no repair procedure developed for this failure mode. Consequently the cracks in the fiber that initiate this failure mode have to be avoided.

As no appropriate experimental data is available to describe the loading limits and the fatigue mechanisms of MFC actuators, the threshold for the maximum allowable strain is derived from customized coupon tests.

Since centrifugal loads and blade bending deformation are the predominant sources of strain the first principal strain occurs parallel to the blade axis and consequently within an angle of 45 ° to the piezoceramic fibers of the MFCs. To reproduce this loading a tension test was chosen. The specimen is made out of the same GFRP that is used for the rotor blade skin and incorporates one MFC actuator at each side to guarantee a symmetric layup. Analog to the relative orientation between piezoceramic fibers and first principle strain in the blade the angle between load direction and piezo fibers was chosen to be 45 ° (see FIGURE 3).

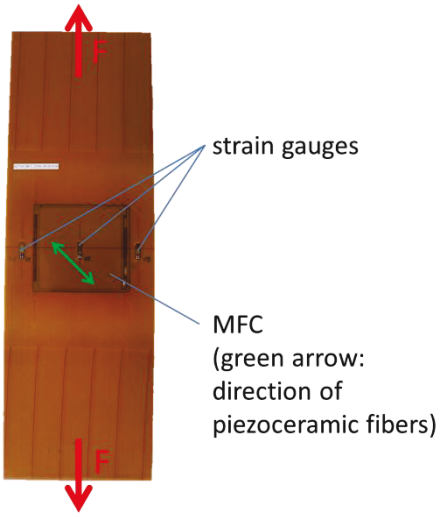

FIGURE 3. Coupon specimen for investigation of failure mechanism and allowable strain

Each specimen was instrumented with 3 strain gages at front and back side to measure the strain that was applied to the actuators. The tests were conducted with a servo hydraulic testing machine allowing static and fatigue loading of the specimen.

Since failure mode 2 is likely to occur at lower load levels and the failure is initiated by cracks in the piezoceramic fibers it was investigated at which load level the cracks occur or start to grow. Therefore the static strain level in the actuators was gradually increased using the servo hydraulic testing machine. At each load step high resolution pictures of the actuators were analyzed to determine the accumulated crack length in a predefined region.

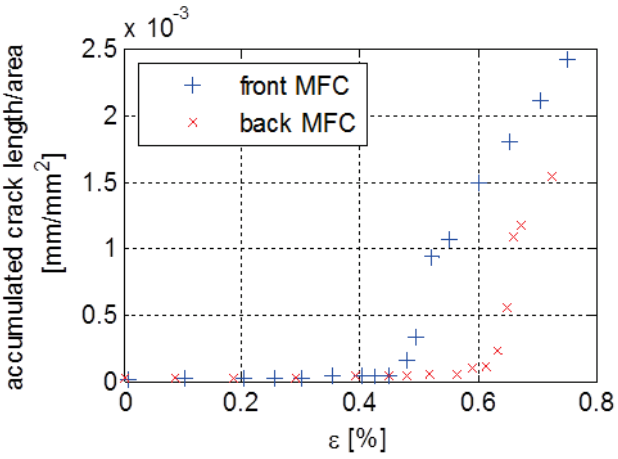

FIGURE 4. Crack growth as a function of strain

FIGURE 4 shows a representative result of the coupon tests. No significant crack initiation or crack growth could be observed below a strain level of 0.45 %. Since this threshold is derived from static tests and as fatigue loading can be expected, a knock-down factor was applied and a strain limit of 0.2 % was used within the design process of the full scale blade. Within the full scale blade segment test the actuators are tested under representative loading conditions and it will be evaluated whether the derived strain limits and the design process described in the next section lead to a robust blade design.

3. BLADE DESIGN

3.1. Design process

There is a multitude of constraints and boundary conditions that make the design of an active twist blade a challenging task. Within the present study an optimization has been used to tackle this challenge.

The goal of the optimization is to find a blade design that meets all constraints with a minimum weight. The constraints are given in TABLE 1.

Parameter	Constraint
Center of gravity	25% chord ± 1%
Torsional stiffness	> 0.7 $GIt_{Reference}$
Active tip twist	± 2°
flap/lag bending stiffness	± 5% $EI_{Reference}$
Elastic axes	± 5% $x_{Reference}$
Strength requirements	

TABLE 1. Optimization constraints

A very detailed parametric finite element model establishes the basis for the investigations. First a sensitivity analysis was performed to identify the parameters that have the highest impact on the objective function and the constraints. In a second step a metamodeling technique was used to optimize the blade structure. The optimized design of the rotor blade only covers the aerodynamic section. Both the blade tip and the blade root are not considered. The parametric finite element model is able to adapt its outer contour to different airfoils. The resulting finite element model is an extrusion of one single cross section that is well suited to determine the blade properties of the investigated cross section. However, the model is not capable to represent the whole blade at once. Hence a strategy to join the results of the optimizations of single cross sections to an optimal overall design had to be developed. Therefore a detailed understanding of the optimization goal and constraints is required. The goal of the optimization was defined to be the mass of the blade that should be minimized with respect to several constraints. The major constraint is the capability to generate a twist rate that enables a blade tip twist of ±2 °. Within this study the twist rate was defined to be constant over the blade span resulting in a linear twist. Further requirements on stiffness, axis positions and strength were converted into optimization constraints as well. This definition of the optimization problem is the key to the developed overall strategy as it minimizes the dependencies between the different cross section optimizations. The twist, stiffness and axis position requirements can be handled separately for each cross section. The strength constraints are the only link between the different optimizations since the mass of the more outboard regions is governing the centrifugal load of the inboard sections. Due to this fact the optimization is starting at the blade tip and then successively approaching the blade root. The accumulated mass is used to estimate the centrifugal load that is used as an input for the strength analysis performed within the optimization. The strategy is visualized in FIGURE 5.

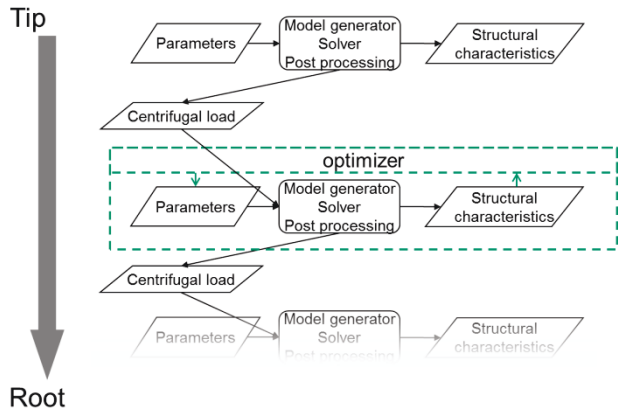

FIGURE 5. Optimization strategy

The optimizer (dashed green box) starts at the tip and is adapting the parameters of the cross section until the constraints are satisfied and a local minimum of the mass of the optimized blade section is found. Subsequently the centrifugal loads for the next section are computed and the optimizer starts optimizing the section located one step further in direction to the blade root.

Within the optimization of the blade the strength is considered using a maximum stress failure criterion for all major load carrying components as well as the actuators. Since a complete rotor simulation including loads computation is not foreseen within this study the torsion and bending moments at ultimate load are assumed to remain unchanged compared to the reference blade even though the blade properties are modified. This simplification significantly reduces the computational effort. Without this assumption it would not be possible to decouple the optimization of the cross sections in the proposed way. A rotor simulation could be performed after the whole blade is optimized. Then the blade optimization process would have to be restarted using the loads derived from the rotor simulation run. This loop would then have to be repeated until convergence is reached.

3.2. Final blade and specimen design

The designed active twist blade features a C-spar, four different airfoils, corresponding blade chords and a parabolic tip. Each optimized blade cross section is composed of seven main components. FIGURE 6 visualizes an arbitrary internal blade configuration.

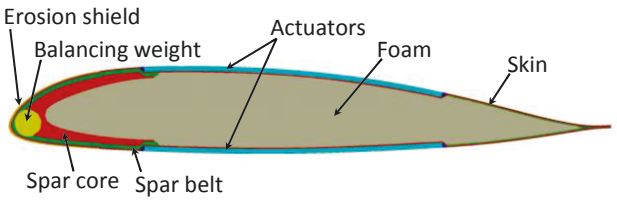

FIGURE 6. General blade design

The final blade design is composed of nine different cross-sections. In general the GFRP skin, which encloses the complete rotor blade, has got a minimal thickness of 0.25 mm. Thus it provides a low torsional stiffness, which is prerequisite for achieving the required twist rate. The skin behind the actuators is extended to a total thickness between 1 mm and 2 mm with layers of CFRP to satisfy the required torsional stiffness and the position of the elastic axis. Due to the higher loads in the root area the thickness of the CFRP layers is slightly higher in these sections. The position of the actuators is located as close as possible to the leading edge, directly behind the erosion shield.

Considering all constraints given in TABLE 1 an increase of blade mass of 19 % compared to the passive reference blade has to be expected. Widening the limits of the constraints can reduce the additional mass dramatically. Ignoring the upper limit of the lead lag stiffness can reduce the increase of blade mass to 15 %. Allowing the torsional stiffness to go down to 60 % of the torsional stiffness of the reference blade, results in an increase of blade mass of 10 % only.

The results from the strength analysis revealed that the cross section with the highest stress in the actuators is located at approx. 40 % of the blade radius. A cross section in this radial range is chosen and simply extruded to obtain the design of the test specimen. Therefore the test specimen has a uniform cross section and no pre-twist. To reduce the costs for the actuators only a small part of the blade span in the middle of the later test section of the specimen was equipped with MFCs. Further on the cross section geometry was slightly modified to reduce the manufacturing effort. Since the finite element model was able to capture these modifications the loads were tuned to obtain a loading condition for the actuators that is equivalent to the optimized active twist blade.

4. SPECIMEN MANUFACTURING

The major components of the blade are depicted in FIGURE 6. The blade skin is divided in an upper and a lower shell. As the skin incorporates the actuators that twist the blade, this is the key-component of the blade segment.

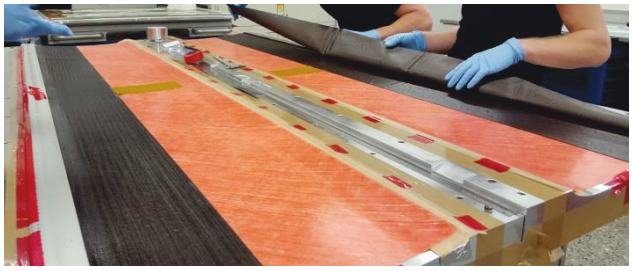

FIGURE 7. Manufacturing of skins

FIGURE 7 gives an impression of the lay-up process of the prepreg skins. The figure shows the lower shell (left) and the upper skin (right) with the integrated actuators, the GFRP layers at the leading edge and the CFRP reinforcement close to the trailing edge.

All composite parts (spar, spar belt and skins) were manufactured in an autoclave process under a pressure of 6 bar at 125 °C.

FIGURE 8. Skin with integrated actuator package

FIGURE 8 depicts the skin with the integrated actuators after the peel ply has been removed. The electrical contacts that were fed through the GFRP prepreg layers are placed with soldering tabs on both sides of the actuator package consisting of three stacked single actuators. On the left and the right side of the actuator the slight changes in color indicate the formation of the staggered transition zone between GFRP and CFRP.

The core of the spar is milled out of a thick spar plate made from GFRP. The foam core that guarantees the stability of the aerodynamic shape in the aft part of the blade is also machined from block material by means of a CNC-mill. In the assembly process skin, spar, spar belts and foam are joined in a closed mold using adhesive films made from thermosetting epoxy resin. Finally the erosion shield that covers the leading edge of the blade segment is bonded using the same thermosetting epoxy resin film as adhesive.

5. TEST BENCH AND INSTRUMENTATION

To test the blade specimen under representative conditions a realistic load collective should be applied. The loading condition of a helicopter blade is rather complex. In contrast to the coupon tests performed to determine the material limits of the MFCs, bending, torsion and axial forces are superimposed during normal operation. This load collective can be reproduced in the developed test bench. A hydraulic cylinder generates an axial force that simulates the centrifugal loads. At the same time a pair of lateral forces applied by a second hydraulic cylinder introduces bending moments in a four point bending configuration. This setup results in a constant bending moment within the test section between the introduction points of the lateral loads. The proportion of lead lag and flap bending can be adjusted by rotating the specimen around its longitudinal axis and thus altering the angle of the attack of the lateral forces with respect to the blade chord line. The appropriate angle has been determined by means of sophisticated three-dimensional numerical finite element analysis.

An electromechanical actuator combined with a pulley setup is used for simultaneous generation of torsion moments. During the test the electromechanical actuator was synchronized with the hydraulic cylinder that applies the blade bending moments in a way that the maximum loads are reached simultaneously. The longitudinal force is kept constant during the tests. Installed in the test bench the model rotor blade is positioned horizontally, with the leading edge (LE) facing down and the trailing edge (TE) pointing upwards. FIGURE 9 gives an overview of the mechanical test setup.

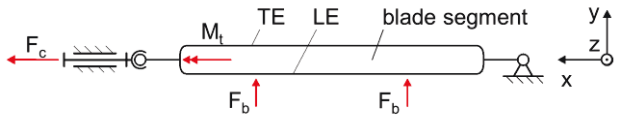

FIGURE 9. Mechanical setup of test rig

At one end the specimen is held by a fixed bearing, allowing only rotation around the z-axis. The other end of the blade is connected to a floating ball joint, enabling rotation around all axes. The ball joint bearing itself can be moved along the x-axis to apply a tension force.

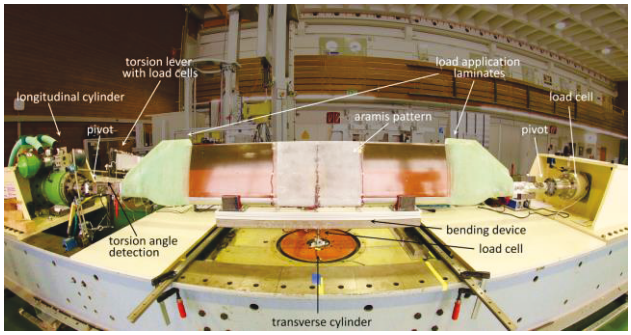

FIGURE 10. Overview of the final test setup

An overview of the final test setup used for both the static and dynamic tests is depicted in FIGURE 10. Whereas the right side of the rotor blade is connected to a 250 kN load cell, the left side is attached to the longitudinal hydraulic cylinder. As both bolt connections allow rotary movements, four point bending loads can be applied by means of the transverse cylinder and a bending device consisting of a beam and two load application supports fitted out with silicone.

A second 20 kN load cell is included in the bending device's push rod connecting the beam and the cylinder via two spherical plain bearings. These are required to allow flap bending displacements and to protect the load cell against bending loads. Furthermore, pure torsional moments can be applied by means of a torsion lever, a rope drive allowing transverse blade movements and an electromechanical actuator. Two 2 kN load cells integrated in the pull ropes are used for the measurement of the torsion moment.

The displacements of the hydraulic cylinders are measured using their internal inductive transducers. Moreover, structural reactions due to torsion are characterized by additional displacement sensors. Whereas inductive displacement transducers are used in the dynamic tests, more precise laser triangulation sensors with a narrow measuring range of ±1 mm are used to determine the much smaller rotations induced by sole active twisting.

Local surface strains due to flap, lag, torsional and tension loads are measured by means of strain gages applied to the top and the bottom skin of the rotor blade. As illustrated in FIGURE 11 and FIGURE 12, a total of eighteen unidirectional strain gages are applied for longitudinal strain determination. The strain gages are located in three longitudinal sections (B, A, C) and in two (B, C) respectively five (A) positions (1-5) along the chord depth. Whereas these gages (quarter bridges) are sensitive to tension, bending and torsion, additional full bridges dedicated to the measurement of bending and torsion moments are applied. The bending moment bridges are wired to be compensated for pure extension, torsion and bending in one direction thus theoretically only being sensitive to bending in the not compensated direction. In the same way, the torsion moment bridges are compensated to detect torsional deformation only.

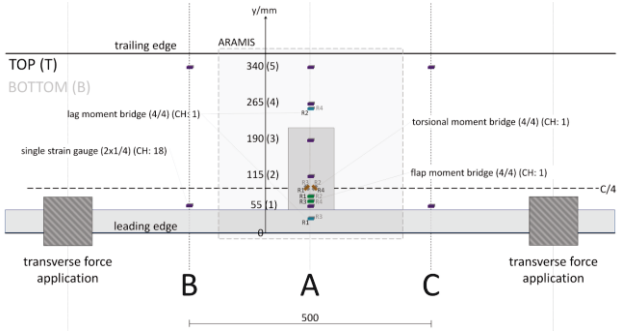

FIGURE 11. Overview of strain gage instrumentation

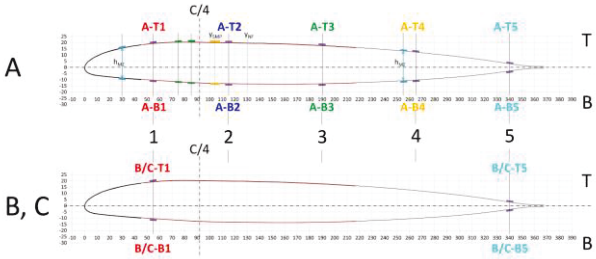

FIGURE 12. Strain gage positions and labels/coloring along chord length

Besides evaluating the global strain field in the uniformly bent part of the rotor blade segment by means of strain gages, optical strain measurement using a stereo camera system is performed. Therefore two ARAMIS systems are used for simultaneous top and bottom surface strain field determination. The area of observation is illustrated in the strain gage application scheme in FIGURE 11 (light gray shaded area). Besides a comparative evaluation of optical and strain gage measurements, the actuator-near strain field is investigated.

6. RESULTS

6.1. Initial active twist performance

For the characterization of the active twist performance the specimen was clamped at one end. At the other end two laser triangulation sensors that were located near the leading and trailing edge of the blade were used to derive the twist deformation generated by the integrated piezoceramic actuators. The actuators are operated with an amplifier that is able to generate -500 V to +1500 V. A signal generator provided a sinusoidal input voltage that is amplified and fed to the actuators. In order to prevent damages of the actuators the voltage range was limited to 70 % of the maximum operation voltage range. This was done in accordance to the expectation that the design target for the active twist performance will be reached within this range.
Within the test the amplitude of the actuation voltage for the actuators was stepwise increased until 70 % of the maximum operation range of the actuators was reached. The maximum achievable twist has been extrapolated.

The actuators were operated separately and in different groups in order to investigate whether their performance can be linearly superposed. The piezoceramic actuators are integrated into three layers of the skin of the rotor blade. As the actuators on the outer surface of the blade are accessible for repair those two were tested until 85 % of the maximum operation voltage range.
FIGURE 13 shows the active twist performance of a full scale blade as a function of the actuator operating voltage range. It is depicted how lower and upper shell actuators contribute uniformly to the total twist. As expected the target tip twist amplitude of ±2 ° can be reached by applying approximately 65 % of the maximum voltage range. This allows operating the actuators at lower voltages and reduces the risk of failures. On the other hand this reveals that the blade weight could be reduced if fewer actuators would be operated at full voltage. The predicted maximum tip twist performance of the blade at full voltage is ±3.63 °. This tip twist amplitude should enable a very efficient noise and vibration attenuation.

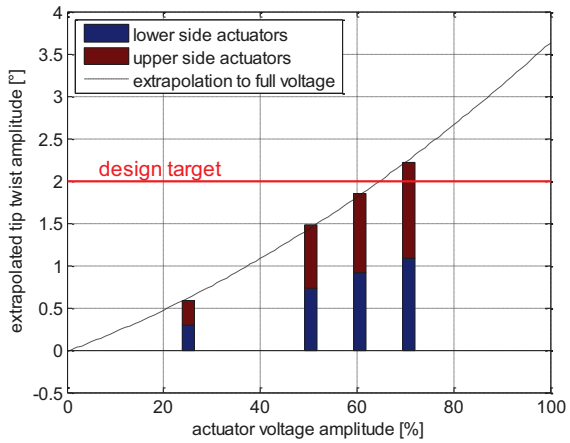

FIGURE 13. Predicted active twist performance of the complete active twist blade

6.2. Blade segment tests

As the representative load combinations applied in the dynamic tests induce rather complex strain fields, strain gage based strain measurement has to be calibrated. Therefore, thorough calibration tests applying pure uniaxial loads (flap bending, lag bending tension and torsion) are conducted to provide a comprehensive understanding of the structural reactions and strain distributions under loading. Besides correlating loads and corresponding strains, the quality of the compensation used in the full bridges for moment measurement is evaluated. To prevent damage of the piezo actuators, maximum strains are kept below 0.1 % in the calibration tests.

While additional test rigs were used for flap and lag bending calibration the specimen was mounted into the test rig for tension and combined tension torsion calibration. Finally the test bench was used to evaluate whether there is fatigue of the actuators and a decrease of their performance under representative loads. During the test the load level was gradually increased in five steps until the final load level given in TABLE 2 was reached. The number of cycles per load level as well as the percentage of the maximum applied load is provided in TABLE 3.

Load	Max.	Min.
Flap Bending Moment [Nm]	850	250
Lag Bending Moment [Nm]	-5800	-1700
Torsion Moment [Nm]	-400	280
Centrifugal Force [kN]	112	112

TABLE 2. Loads at highest load stage

Load stage	% max. load	cycles
1	10	10000
2	25	25000
3	50	50000
4	75	85000
5	100	100000
sum		270000

TABLE 3. Load stages and cycles

In order to assess the active twist performance different indicators can be used. Actuator voltage, current and capacity can be used to check the electrical properties of the MFC. An electrical break down or a depolarization of the piezoceramic material can be monitored using these electrical quantities. The transducer characteristic of the piezoelectric material also enables to detect a mechanical degradation of the MFC but the sensitivity is expected to be low. To assess the mechanical performance of the actuators it would be favorable to use a setup equivalent to the initial characterization of the active twist performance in section 6.1. Unfortunately it would result in an enormous effort to unmount and reinstall the blade from and into the test stand. A compromise was found by unmounting the torsion application mechanism and characterization of the blade at a small axial tension load of 0.2 kN. Using this setup the friction that has to be overcome by the actuators is quite low. On the other hand the generated twist angle is also small since only a small section of the specimen is equipped with actuators. Besides measuring the twist angle the strain gage bridge for the detection of the torsion moment that is directly located on top of the actuators could also be a good indicator for the locally generated strains. As a consequence of the blades torsional elasticity the influence of friction on the strain gage signals is expected to be smaller than on the direct measurement of the twist angle. But since the strain gages are also subjected to a cyclic loading at strain up to 0.2 % a fatigue of the strain gages themselves cannot be excluded.

The characterization of the active twist was performed each 10000 cycles and each time the cyclic testing was interrupted.

FIGURE 14 shows the active twist angles measured over the course of the test. The diagram was generated post processing the data of the laser triangulation sensors.

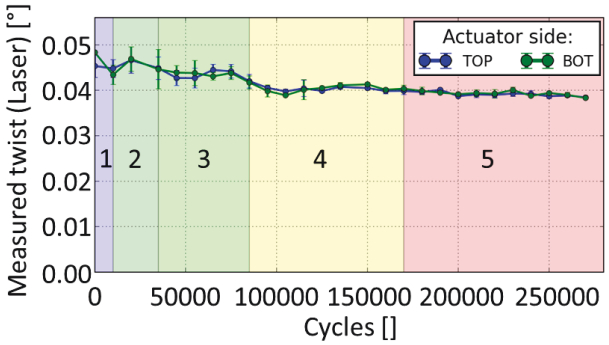

FIGURE 14. Active performance - twist angle

The graph shows some minor decrease of approx. 10 % in measured twist over the first three load stages. In the range from 100.000 cycles up to the end of the test at 270.000 cycles the measured twist scatters around a constant value. Due to the high repeatability of the characterization runs the error bars are almost invisible behind the markers. The fact that the performance rather seems to diminish in the range of small load levels than to decrease at higher loading leads to the assumption that this could be a phenomenon caused by settling in the test bench or the specimen.

The post processing of the local strains detected with the strain gage bridge for torsion moment measurement could confirm the results of the twist angle measurements.

In contrast to that the electrical indicators, current and capacity did not show any decrease over the whole test campaign.

Finally it can be stated that despite the intensive testing the MFCs did neither fail in mode 1 nor in mode 2. This emphasizes that both the chosen material limits as well as the design process were conservative and resulted in a robust design of an active twist blade that can withstand the rough environment of the main rotor of a helicopter.

7. CONCLUSION

After determining the material limits of the used piezoelectric actuators in customized coupon tests, these limits are used within the optimization process to derive the design of a full scale active twist blade. A representative section was selected and a test specimen was manufactured.

The main objective of the experimental test program is to investigate the impact of combined dynamic biaxial bending, in phase dynamic torsion and constant tension on active twist performance.

Although the experimentally observed active twist angles are rather small due the fact that only a small region of the specimen is equipped with actuators, extrapolation reveals that the design target (2 ° tip twist angle) could be met in case of a fully-equipped blade. This even holds true for medium electrical actuator loads of about 65 % of the maximum voltage.

Before testing, single longitudinal strain gages and full bridges dedicated to the measurement of moments (flap bending, lag bending and torsion) are applied.

Within the dynamic tests series, five load levels and a total of 270.000 cycles are tested. In contrast to operational application, active twisting is not performed together with simultaneous external loading due to safety reasons. Instead, active performance is characterized in an interval of 10.000 cycles of continuous dynamic testing. Besides twisting angle, local torsion bridge strain, piezo stack current and electric capacitance are evaluated. Although twisting angle and corresponding strains are observed to decrease slightly with growing cycle number, this most likely is due to wear and friction of the hinges used for load application. Overall, there is no evidence that twisting performance is affected by representative dynamic operational loads in an order of magnitude that cannot be easily compensated using the available margin in operating voltage of the actuators.

ACKNOWLEDGEMENT

The work in this paper is supported by the Clean Sky Joint Technology Initiative (grant number CSJU-GAM-GRC-2008-001) – GRC1 Innovative Rotor Blades, which is part of the European Union 7th Framework Program (FP7/2007-2013).

REFERENCES

[1] Chapter 1 Sources of Vibrations. In: Krysinski, T. ; Malburet, F.: Mechanical Vibrations - Active and Passive Control. London : ISTE Ltd., 2007. ISBN 978-1-905209-29-3

[2] Chapter 17 Noise. In: Johnson, W.: Helicopter theory. Dover Publications, 1994. ISBN 0-486-68230-7

[3] Chapter 12-5 Vibration and Loads. In: Johnson, W.: Helicopter theory. Dover Publications, 1994. ISBN 0-486-68230-7

[4] Körber, S. ; Ballmann, J.: Mechanisms and acoustics of Blade-Vortex-Interactions. In: Z. Flugwiss. Weltraumforsch. 19 (1995), p. 397-406

[5] Wierach, P. ; Riemenschneider, J. ; Opitz, S. ; Hoffmann, F.: Experimental Investigation of an Active Twist Model Rotor Blade under Centrifugal Loads. In: Proceedings of the 33rd European Rotorcraft Forum. Kazan, Russia, 2007

[6] Booth, E. R. ; Wilbur, M. L.: Acoustic aspects of active-twist rotor control. In: American Helicopter Society 58th Annual Forum. Montreal, Canada, 2002

[7] Sekula, M. K. ; Wilbur, M. L. ; Yeager, W. T.: Aerodynamic Design Study of an Advanced Active Twist Rotor. In: Proceedings of the American Helicopter Society 4th Decennial Specialist's conference on Aeromechanics. San Francisco, USA, 2004

[8] van der Wall, B.G.: Der Einfluss aktiver Blattsteuerung auf die Wirbelbewegung im Nachlauf von Hubschrauberrotoren, Technische Universität Carolo-Wilhelmina zu Braunschweig, PHD-thesis, 1999

[9] Müller, M. ; Arnold, U. T. P. ; Morbitzer, D.: On the importance and the ectiveness of 2/rev IBC for noise, vibration and pitch link load reduction. In: Proceedings of the 25th European Rotorcraft Forum. Rome, Italy, 1999

[10] Derham, R. ; Weems, D. B. ; Mathew, M. B. ; Bussom, R. C.: The design evolution of an active materials rotor. In: Proceedings of the American Helicopter Society 57th Annual Forum. Washington DC, USA, 2001

[11] Shin, S. ; Cesnik, C. E. S. ; Hall, R: Closed-Loop Control Test of the NASA/ARMY/MIT Active Twist

Rotor for Vibration Reduction. In: Proceedings of the American Helicopter Society 59th Annual Forum. Phoenix, USA, 2003
[12] Wilbur, M. L. ; Mirick, P. H. ; Yeager, W. T. ; Langston, C. L. ; Cesnik, C. E. S. ; Shin, S.: Vibratory Loads Reduction Testing of the NASA/ARMY/MIT Active Twist Rotor. In: Proceedings of the American Helicopter Society 57th Annual Forum. Washington DC, USA, 2001
[13] Wilbur, M. L. ; Yeager, W. T. ; Sekula, M. K.: Further examination of the vibratory loads reduction results from the NASA/ARMY/MIT active twist rotor test. In: Proceedings of the American Helicopter Society 58th Annual Forum. Montreal, Canada, 2002
[14] Riemenschneider, J. ; Opitz, S. ; Wierach, P. ; Rochettes, H. M. ; Buchaniek, L. ; Joly, D.: Structural Design and Testing of Active Twist Blades - a Comparison. In: Proceedings of the 35th European Rotorcraft Forum. Hamburg, Germany, 2009
[15] Wierach, P. ; Riemenschneider, J. ; Opitz, S. ; Hoffmann, F.: Experimental Investigation of an Active Twist Model Rotor Blade under Centrifugal Loads. In: Proceedings of the 33rd European Rotorcraft Forum. Kazan, Russia, 2007
[16] Monner, H.P. ; Opitz, S. ; Riemenschneider, J. ; Wierach, P.: Evolution of Active Twist Rotor Designs at DLR. In: Proceedings of the 16th AIAA/ASME/AHS Adaptive Structures Conference. Schaumburg, USA, 2008
[17] Opitz, S. ; Riemenschneider, J. ; Monner, H. P.: Modal Investigation of an Active Twist Helicopter Rotor Blade. In: Proceedings of the ICAST - International Conference on adaptive Structures and Technologies. Hong Kong, China, 2009
[18] Opitz, S. ; Riemenschneider, J.: Measurement of the dynamic tip twist angles of an Active Twist model scale rotor blade. In: Proceedings of the 36th European Rotorcraft Forum. Paris, France, 2010
[19] Weems, D. B. ; Anderson, D. M. ; Mathew, M. B. ; Bussom, R. C.: A Large-Scale Active-Twist Rotor. In: Proceedings of the American Helicopter Society 60th Annual Forum. Baltimore, USA, 2004
[20] Deraemaeker, A. ; Nasser, H. ; Benjeddou, A. ; Preumont, A.: Mixing rules for Macro Fiber Composites (MFC). In: Journal of Intelligent Material Systems and Structures, 2009, Vol20
[21] Wierach, P.: Low profile piezo actuators based on multilayer technology. In: Proceedings of the 17th International Conference on Adaptive Structures and Technologies. Taipei, Taiwan, 2006
[22] Wierach, P. ; Hennig, E. ; Ditas, P. ; Linke, S.: Piezocomposite actuators based on multilayer technology. In: Proceedings of the International Symposium on Piezocomposite Application ISPA. Dresden, Germany, 2009
[23] Wierach, P. ; Opitz, S. ; Kalow, S.: Experimental investigation of an active twist model rotor blade with a low voltage actuation system. In: The Aeronautical Journal, December 2015, Volume 119, no 1222, p.1499-1512